THE SPIRAL CONFIGURATION OF SUNSPOT MAGNETIC FIELDS

M. J. HAGYARD, E. A. WEST, and N. P. CUMINGS
*Space Sciences Laboratory, ES*13, *NASA-Marshall Space Flight Center, Alabama* 35812, *U.S.A.*

(Received 8 November; in revised form 20 December, 1976)

Abstract. Distributions of circularly and linearly polarized intensities are computed using an analytical magnetic field model for an isolated sunspot, and these intensity distributions are compared with observed intensities in all Stokes parameters in the λ 5250 line measured with the Marshall Space Flight Center's vector magnetograph. The qualitative agreement between measured and calculated linearly polarized intensity distributions is discussed with regard to implications as to the configuration of the transverse magnetic field of the isolated sunspot.

1. Introduction

In early 1976 an extensive effort to optimize the Marshall Space Flight Center's magnetograph system was completed, and the operation of the instrument to measure transverse magnetic fields was initiated. A description of this magnetograph can be found in the NASA publication 'Real Time Solar Magnetograph Skylab Mission Atlas' (Hagyard and Cumings, 1975). Although the final calibration of the vector magnetograph has just been completed, preliminary measurements of linearly polarized intensities in the λ 5250 line have been made for several active regions over the past 6 months. Of particular interest are data obtained for the large sunspot which was on the disk during the period 21 April to 3 May, 1976, Boulder number 700. On 27 April when the spot was at disk center (and at 9° south heliographic latitude), Polaroid pictures were obtained showing the distributions of circularly and linearly polarized intensities over the umbra and penumbra of this spot; see Figures 1 and 2. In this paper we present a theoretical calculation of polarized intensity distributions which would be measured by our magnetograph system using an analytical model for the vector magnetic field of an isolated sunspot, and we compare these calculations with the observed data for 27 April.

2. Theoretical Sunspot Model

The model of the vector magnetic field distribution which we considered initially is the axisymmetric solution for a force-free magnetic field as developed by Nakagawa *et al.* (1971). In cylindrical coordinates the field components are given by

$$B_r = B_0 \cos \tau J_1(kr) e^{-\beta z}, \tag{1a}$$

$$B_\theta = B_0 \sin \tau J_1(kr) e^{-\beta z}, \tag{1b}$$

$$B_z = B_0 J_0(kr) e^{-\beta z}, \tag{1c}$$

where τ is the angle between the transverse (B_r, B_θ) component of the magnetic

Solar Physics **53** (1977) 3–13.

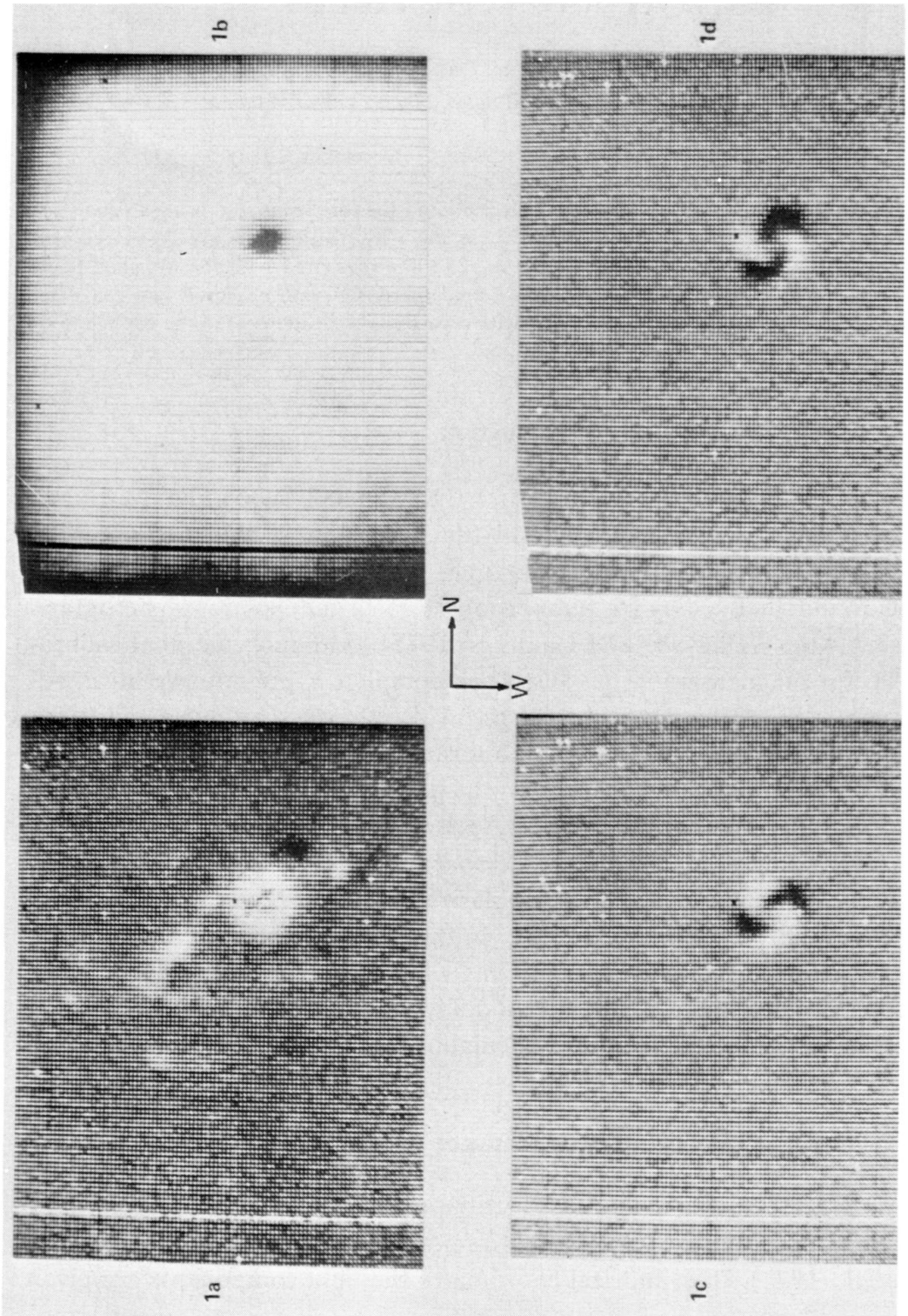

Fig. 1. Linearly and circularly polarized intensity distributions for sunspot (Boulder Number 700) at disk center on 27 April 1976. Field of view is 5×5 arc minute. (a) Circularly polarized intensity. (b) Picture of spot. (c) Linearly polarized intensity ∥ and ⊥ to analyzer. (d) Linearly polarized intensity at 45° and 135° to analyzer.

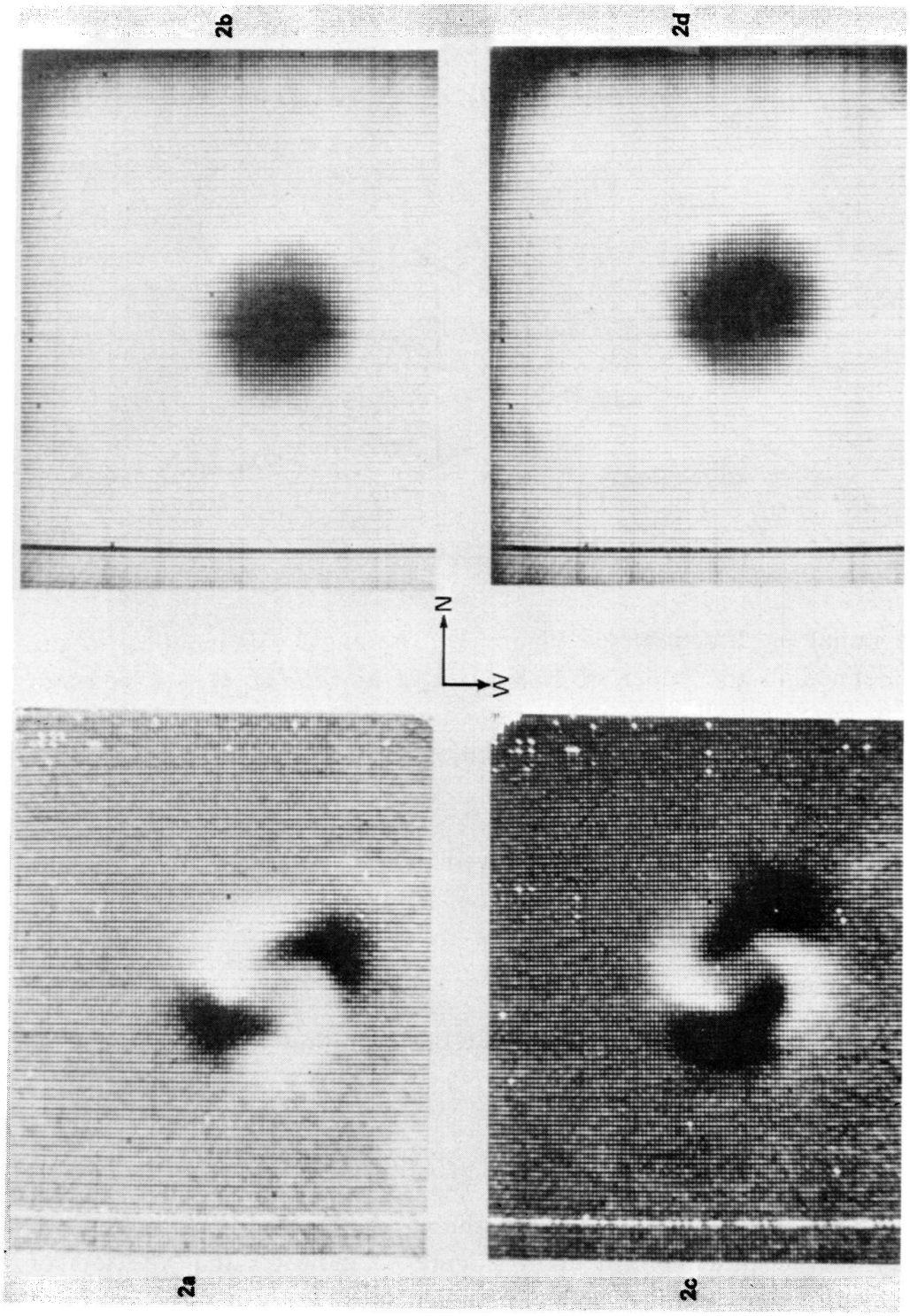

Fig. 2. High magnification (2.5×2.5 arc minute field of view) of linearly polarized intensities. (a) Linearly polarized intensity ∥ and ⊥ to analyzer. (b) Corresponding picture of spot. (c) Linearly polarized intensity at 45° and 135° to analyzer. (d) Corresponding picture of spot.

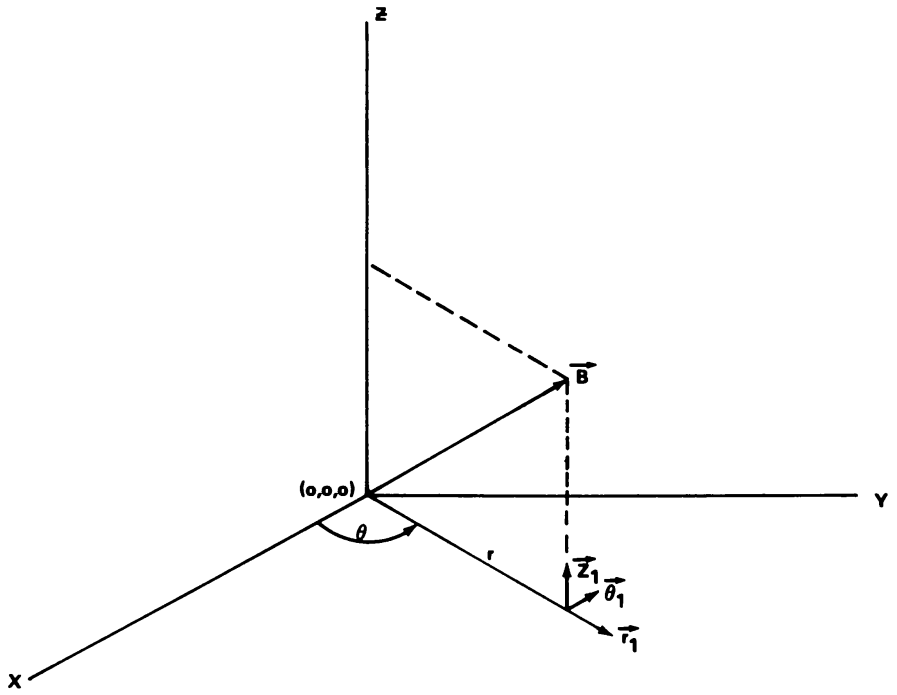

Fig. 3. Cylindrical coordinate geometry.

field and the radial (r) direction (see Figure 3). The angle τ is identical to the spiral angle defined in the paper of Nakagawa *et al.* (1971); it is a constant independent of space coordinates.

These equations represent the simplest solution to the force-free condition

$$\nabla \times \mathbf{B} = \alpha \mathbf{B} \tag{2}$$

for constant α and a z-dependence of $\mathbf{B}$ given by $e^{-\beta z}$, where β^{-1} is the scale height of the magnetic field. The parameter k found in the arguments of the Bessel functions $J_1(kr)$ and $J_0(kr)$ is given by

$$k^2 = \alpha^2 + \beta^2 ; \tag{3}$$

it is numerically defined in our calculations by the condition

$$J_1(kR_m) = 0$$

for $kR_m = 3.8317$, where R_m is the maximum value of r.

This solution was considered because of the spiral pattern formed by the projected three-dimensional field lines as shown in Figure 4. A qualitative analysis of a general spiral configuration (Figure 5) indicates that the loci of transverse field directions parallel and perpendicular to a given direction form patterns similar to the 'pinwheels' seen in the transverse field observations (Figures 1 and 2). However, a simple analysis shows that the spiral pattern of the force-free solution will not yield the desired results. The angle ϕ that the transverse field makes with an arbitrary x-axis is given by (see Figure 6)

$$\tan \phi = B_y / B_x .$$

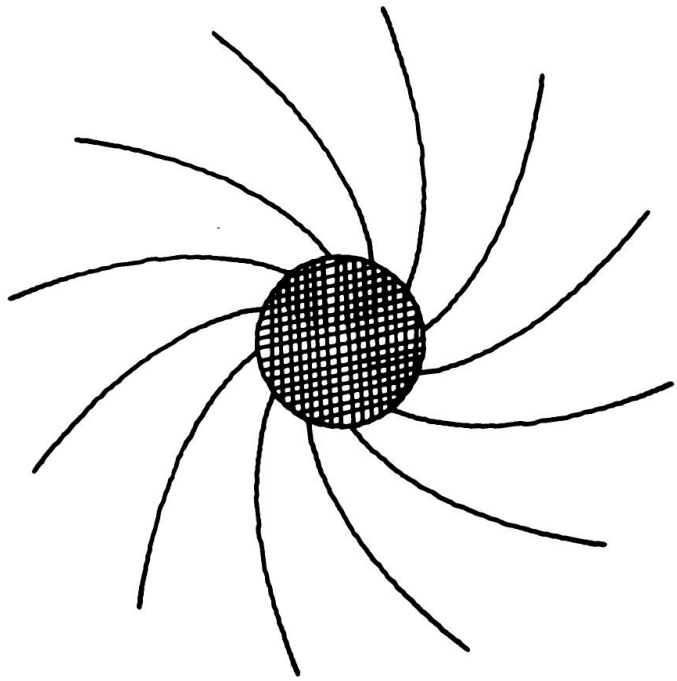

Fig. 4. Projected field lines for force-free magnetic field.

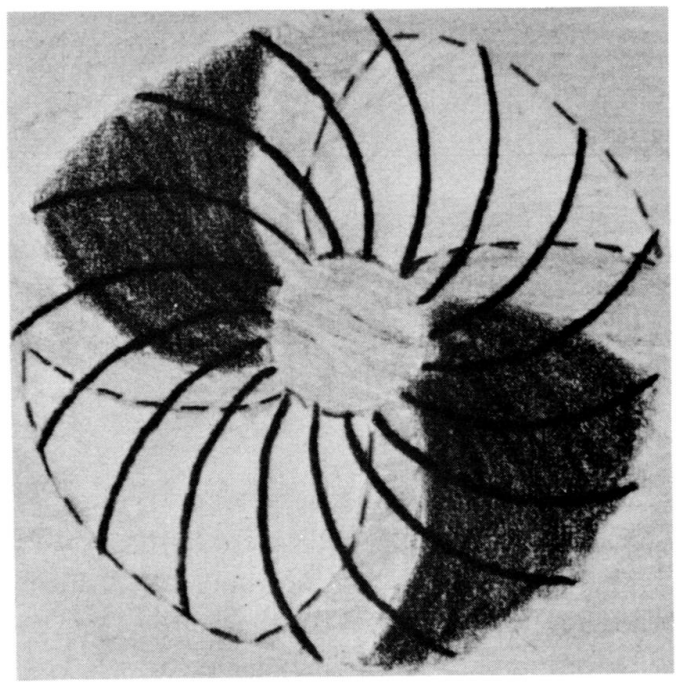

Fig. 5. Schematic distribution of loci of transverse field directions || and ⊥ to analyzer.

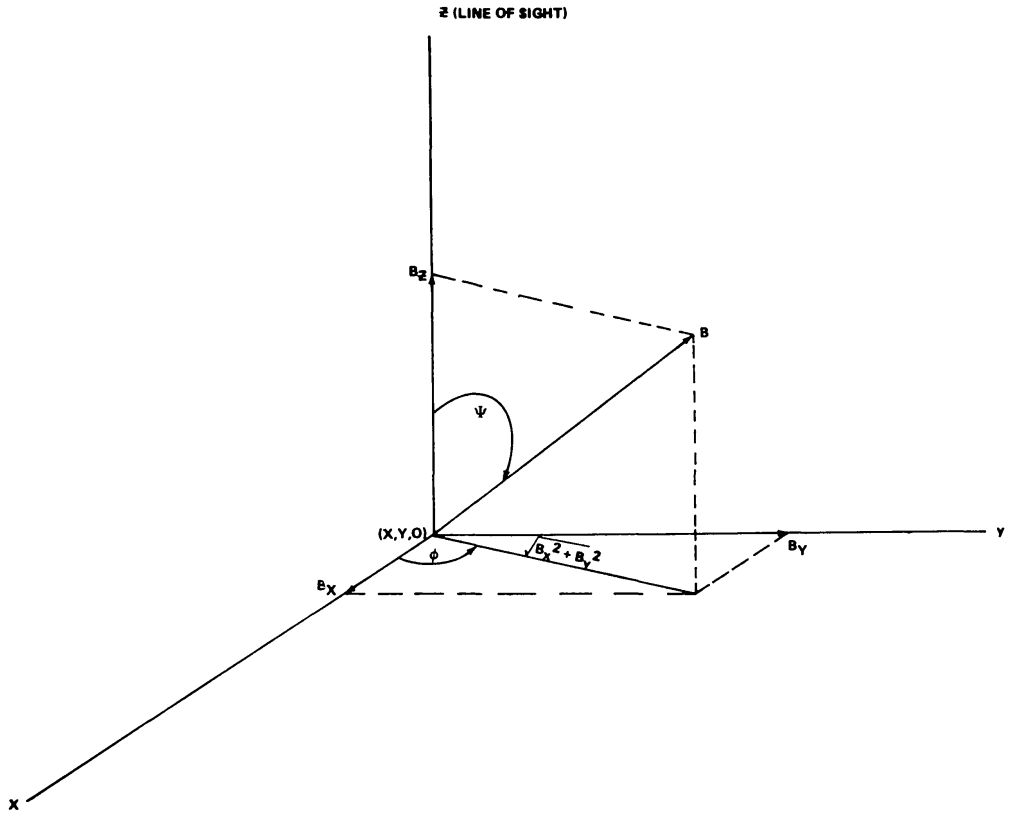

Fig. 6. Vector magnetic field geometry.

The necessary transformations from cylindrical to rectangular coordinates give

$$B_x = B_r \cos\theta - B_\theta \sin\theta \tag{4}$$

and

$$B_y = B_r \sin\theta + B_\theta \cos\theta\ ; \tag{5}$$

then

$$\tan\phi = \tan(\theta + \tau)$$

or

$$\phi = \theta + \tau\,.$$

Since the spiral angle τ is a constant independent of the space coordinates (r, θ, z), the points at which the transverse field orientation ϕ is the same lie along the *radial* direction given by $\theta = \phi - \tau = \text{constant}$, and the resulting intensity patterns will not exhibit the observed spirals. Consequently, we consider an analytic magnetic field configuration (*not* force-free) given by

$$B_r = B_0 J_1(kr) e^{-\beta z}\,, \tag{6}$$

$$B_\theta = B_0 (r/R) J_1(kr) e^{-\beta z}\,, \tag{7}$$

$$B_z = B_0 J_0(kr) e^{-\beta z}\ ; \tag{8}$$

it can be verified readily that the equation for the transverse field lines is identical to that for the Archimedes' spiral, $r = R\theta$. For the purposes of our calculations we take the solutions for the case $z = 0$ everywhere and we are interested in the quantities

$$B = (B_x^2 + B_y^2 + B_z^2)^{1/2}, \tag{9}$$

$$\psi = \tan^{-1}[(B_x^2 + B_y^2)^{1/2}/B_z], \tag{10}$$

$$\phi = \tan^{-1}(B_y/B_x). \tag{11}$$

3. Calculation of Emerging Intensities

The circularly and linearly polarized intensities of a Zeeman sensitive absorption line formed in the presence of a magnetic field can be expressed in terms of the Stokes parameters, I, Q, U, and V. We took as our solution to the radiative transfer equations for the Stokes parameters the simple analytical form derived by Unno (1956) assuming a homogenous field, pure absorption, and a Milne–Eddington atmosphere. Since we have assumed our vector magnetic field lies in the $z = 0$ plane, the model adopted earlier in Section 2 is consistent with the assumption of a homogenous magnetic field. The emerging intensities I, Q, and V as well as the continuum intensity I_0 are then given by

$$I = A\left[1 + \beta_0\mu\left(\frac{1+\eta_I}{D}\right)\right], \tag{12}$$

$$I_0 = A[1 + \beta_0\mu], \tag{13}$$

$$Q = -A\beta_0\mu(\eta_{Q/D}), \tag{14}$$

$$V = -A\beta_0\mu(\eta_{V/D}), \tag{15}$$

where

$$D = (1+\eta_I)^2 - (\eta_Q^2 + \eta_V^2) \tag{16}$$

and

$$\eta_I = \frac{\eta_p}{2}\sin^2\psi + \left(\frac{\eta_r + \eta_l}{4}\right)(1+\cos^2\psi), \tag{17a}$$

$$\eta_Q = \left(\frac{\eta_p}{2} - \frac{\eta_r + \eta_l}{4}\right)\sin^2\psi, \tag{17b}$$

$$\eta_V = \left(\frac{\eta_r - \eta_l}{2}\right)\cos\psi. \tag{17c}$$

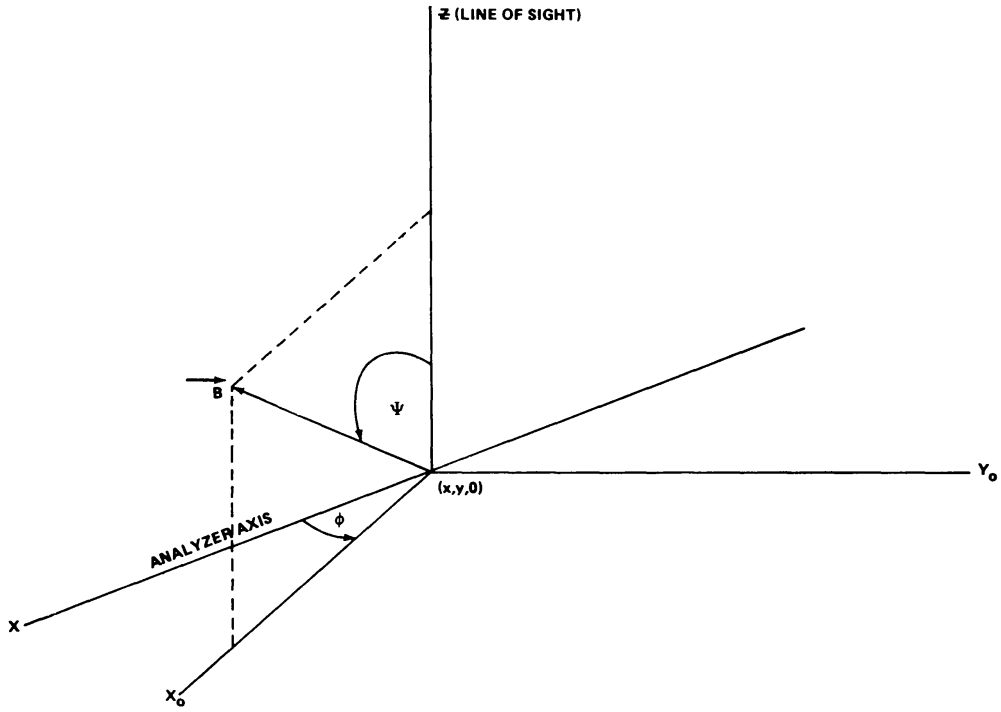

Fig. 7. Unno coordinate system (X_0, Y_0, Z).

The η_p, η_r, and η_l are the ratios of line-to-continuous absorption coefficients for the central and two split Zeeman components; we have assumed they are given by

$$\eta_p = \eta_0 H(\lambda)\,, \tag{18a}$$

$$\eta_r = \eta_0 H(\lambda + \Delta\lambda_B)\,, \tag{18b}$$

and

$$\eta_l = \eta_0 H(\lambda - \Delta\lambda_B)\,, \tag{18c}$$

where η_0 is a constant, H is the normalized Voigt profile, and $\Delta\lambda_B$ gives the Zeeman wavelength splitting. In the coordinate system (X_0, Y_0, Z) defined in the Unno paper, the fourth Stokes parameter U is zero for a homogenous magnetic field; this coordinate system is illustrated in Figure 7. The parameters β_0 and μ are the limb darkening coefficient and disk position, respectively.

4. Theoretical Magnetograph Measurements

The Marshall Space Flight Center vector magnetograph measures circularly polarized intensities in the 'longitudinal' mode which produces an image of intensities proportional to the line-of-sight component of the magnetic field; this image is referred to as 1AB. In the 'transverse' mode, linearly polarized intensities are measured in two directions separated by 45°, and the corresponding images are designated 2AB and 3AB. In order to reduce the possibility of 'cross-talk' between the circularly polarized intensity and the weaker linear

components, we make our transverse measurements (2AB, 3AB) with the magnetograph's $\frac{1}{8}$ Å Zeiss birefringent filter tuned to the center of the 5250.22 Å absorption line. For the longitudinal measurement (1AB) the filter is tuned 60 mÅ into the blue wing of the line. Relating the polarized intensities 1AB, 2AB, and 3AB to those of the Stokes parameters, we have

$$1\text{AB} \sim \overline{(V/I_0)}/\overline{(I/I_0)}\,, \tag{19}$$

$$2\text{AB} \sim [\overline{(Q/I_0)}/\overline{(I/I_0)}] \cos 2\phi\,, \tag{20}$$

$$3\text{AB} \sim [\overline{(Q/I_0)}/\overline{(I/I_0)}] \sin 2\phi\,, \tag{21}$$

where ϕ represents the angle between the transverse component of **B** and the analyzer axis of the magnetograph as shown in Figure 7; it should be noted that this is identical to the angle ϕ in Figure 6. The quantities $\overline{(V/I_0)}/\overline{(I/I_0)}$ and $\overline{(Q/I_0)}/\overline{(I/I_0)}$ are the circular and linear Stokes parameters averaged over the bandpass of the Zeiss birefringent filter:

$$\overline{(V/I_0)}/\overline{(I/I_0)} = \frac{\int_{\text{bandpass}} (\text{filter profile}) \times (V/I_0)\, d\lambda}{\int_{\text{bandpass}} (\text{filter profile}) \times (I/I_0)\, d\lambda} \tag{22}$$

and

$$\overline{(Q/I_0)}/\overline{(I/I_0)} = \frac{\int_{\text{bandpass}} (\text{filter profile}) \times (Q/I_0)\, d\lambda}{\int_{\text{bandpass}} (\text{filter profile}) \times (I/I_0)\, d\lambda}\,. \tag{23}$$

Thus, using the analytic magnetic field model, we derive at each point $(x, y, 0)$ in the sunspot the value B which determines the Zeeman splitting ($\Delta\lambda_B \sim B$), ψ which determines the parameters η_I, η_Q and η_V, and ϕ which is used to calculate the intensities of 2AB and 3AB. The 'pictures' 1AB, 2AB, and 3AB are then generated using the Unno solutions with the following parameters:

$\beta_0 = 2.00$,
$\eta_0 = 10.0$,
damping constant $= 0.10$,
$\mu = 1.00$,
Doppler width $= 35$ mÅ.

5. Results and Conclusions

Theoretical 'magnetograms' (1AB, 2AB, and 3AB) were generated for the case $B_0 = 1000$ gauss and the Archimedes' spiral parameter $R = \frac{1}{2}R_m$; the results for the linear polarization are shown in Figure 8. In comparing these with the observed patterns (Figure 2) one can see the qualitative agreement between the

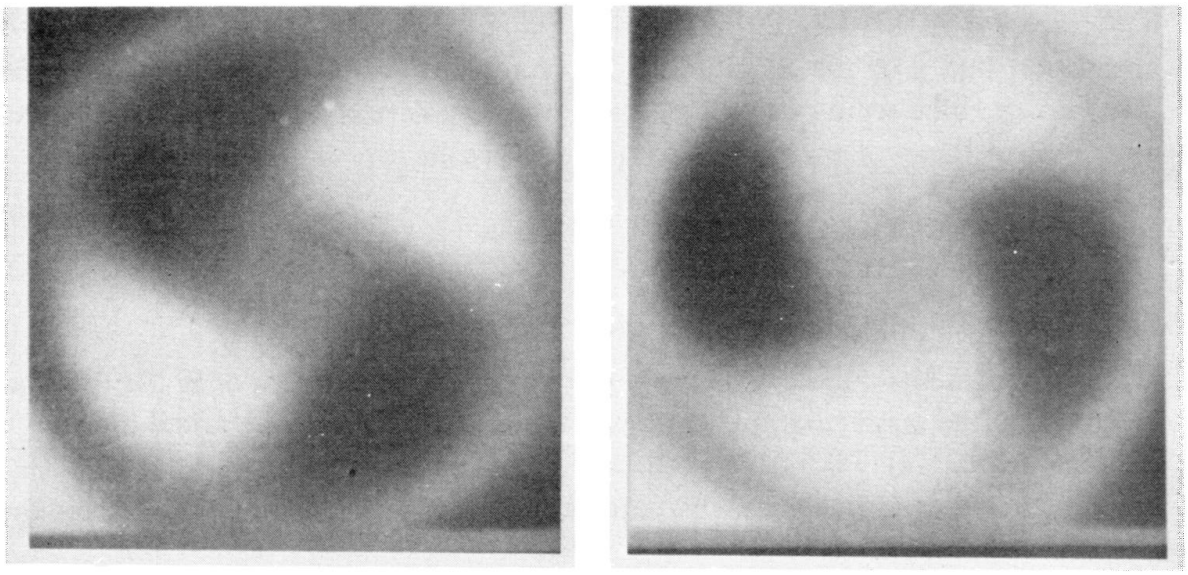

A B

Fig. 8. Theoretical calculations of linearly polarized intensity distributions. (A) 2AB; (B) 3AB.

theoretical model and the observations for the transverse fields. However, the model fails to represent the observed circular polarization patterns which show a region of strong positive polarity and isolated regions of weaker negative polarity (Figure 1). On the other hand, for the longitudinal mode, the model gives a circularly symmetric pattern of a strong positive core surrounded by a ring of (weaker) negative polarity. This failure of the model for the longitudinal fields is an indication of the simplistic nature of our model.

If we accept these results on the basis of the agreement for the transverse fields, we are led to the conclusion that these fields are neither potential nor force-free with constant α; for photospheric fields this is not a startling conclusion. In the case of the force-free model, the indication is that α is not constant, since a constant angle of 'twist', τ, will not produce the observed results, and α and τ are related via the equation

$$\tan\tau = \alpha/\beta$$

in the model of Nakagawa *et al.* (1971).

The transverse field configuration reported in this paper seems to be a fairly typical one for simple, isolated sunspots since we have observed these 'pinwheel' patterns in four other large sunspots; Table I summarizes these observations. Because of the small number of examples we do not find the correlation between solar cycle and spiral configuration to be statistically meaningful at this time. In future research we intend to study the evolution of these patterns throughout the lifetime of a sunspot by directly calculating the vector field configurations from the data.

TABLE I
Summary of observed sunspots with spiral configurations

Date	Boulder number	Coordinates	Solar cycle	Spiral configuration
19 April 1976	697	N05E08	old	clockwise
27 April 1976	700	S09W01	old	clockwise
12 May 1976	704	N01W10	old	clockwise
01 October 1976	742	N16W06	new	counterclockwise
21 November 1976	757	N12E05	new	counterclockwise

Acknowledgements

We would like to express our appreciation for useful discussions with Dr Neil Sheely of the Naval Research Laboratory concerning the transverse data. We are also very grateful to Dr E. Tandberg-Hanssen for reading this manuscript and for his continued encouragement and interest in the MSFC magnetograph project. Finally, we thank the referee for his constructive comments concerning this paper.

References

Hagyard, M. J. and Cumings, N. P.: 1975, NASA TM X-64922.
Nakagawa, Y., Raadu, M. A., Billings, D. E., and McNamara, D.: 1971, *Solar Phys* **19,** 72.
Unno, W.: 1956, *Publ. Astron. Soc. Japan* **8,** 108.